Journal of Orthopaedic Translation 46 (2024) 65–78

Contents lists available at ScienceDirect

Journal of Orthopaedic Translation

journal homepage: www.journals.elsevier.com/journal-of-orthopaedic-translation

Original Article

HIF-2α/TFR1 mediated iron homeostasis disruption aggravates cartilage endplate degeneration through ferroptotic damage and mtDNA release: A new mechanism of intervertebral disc degeneration

Xingzhi Jing [a,1], Wenchao Wang [a,1], Xining He [b], Xiaoyang Liu [a], Xiaoxia Yang [a], Cheng Su [a], Yuandong Shao [c], Zhongpeng Ge [a], Heran Wang [d], Xingang Cui [a,*]

[a] Department of Spine Surgery, Shandong Provincial Hospital Affiliated to Shandong First Medical University, Jinan, 250000, China
[b] Department of Neurosurgery, Binzhou People's Hospital, Binzhou, 256600, China
[c] Department of Spine Surgery, Binzhou People's Hospital, Binzhou, 256600, China
[d] Department of Spine Surgery, Shandong Provincial Hospital, Shandong University, Jinan, 250000, China

ARTICLE INFO

Keywords:
cGAS-STING
Iron metabolism
Intervertebral disc degeneration
mtDNA
TfR1

ABSTRACT

Backgroud: Iron overload is a prevalent condition in the elderly, often associated with various degenerative diseases, including intervertebral disc degeneration (IDD). Nevertheless, the mechanisms responsible for iron ion accumulation in tissues and the mechanism that regulate iron homeostasis remain unclear. Transferrin receptor-1 (TFR1) serves as the primary cellular iron gate, playing a pivotal role in controlling intracellular iron levels, however its involvement in IDD pathogenesis and the underlying mechanism remains obscure.

Methods: Firstly, IDD mice model was established to determine the iron metabolism associated proteins changes during IDD progression. Then CEP chondrocytes were isolated and treated with TBHP or pro-inflammatory cytokines to mimic pathological environment, western blotting, immunofluorescence assay and tissue staining were employed to explore the underlying mechanisms. Lastly, TfR1 siRNA and Feristatin II were employed and the degeneration of IDD was examined using micro-CT and immunohistochemical analysis.

Results: We found that the IDD pathological environment, characterized by oxidative stress and pro-inflammatory cytokines, could enhance iron influx by upregulating TFR1 expression in a HIF-2α dependent manner. Excessive iron accumulation not only induces chondrocytes ferroptosis and exacerbates oxidative stress, but also triggers the innate immune response mediated by c-GAS/STING, by promoting mitochondrial damage and the release of mtDNA. The inhibition of STING through siRNA or the reduction of mtDNA replication using ethidium bromide alleviated the degeneration of CEP chondrocytes induced by iron overload.

Conclusion: Our study systemically explored the role of TFR1 mediated iron homeostasis in IDD and its underlying mechanisms, implying that targeting TFR1 to maintain balanced iron homeostasis could offer a promising therapeutic approach for IDD management.

The translational potential of this article: Our study demonstrated the close link between iron metabolism dysfunction and IDD, indicated that targeting TfR1 may be a novel therapeutic strategy for IDD.

1. Introduction

Intervertebral disc degeneration (IDD) is a leading cause of lower back pain (LBP) and associated with lumbar disorders, making a substantial contribution to human disability and global health burdens. To date, effective treatment strategies for IDD are lacking, with surgery and pain relief medications being the primary options [1]. Consequently, further research is essential to elucidate the underlying mechanisms of IDD development and progression, and identify new treatment targets. IDD has a complex etiology, arising from the interplay of various risk factors, including aging, osteoporosis, mechanical stress, inflammation, and metabolic abnormalities [2]. Nonetheless, the specific

* Corresponding author. Department of spine surgery, Shandong Provincial Hospital Affiliated to Shandong First Medical University, Jinan, Shandong, 250021, China.
E-mail address: cuixingang@sdfmu.edu.cn (X. Cui).
[1] These authors contributed equally to this work

https://doi.org/10.1016/j.jot.2024.03.005
Received 25 December 2023; Received in revised form 22 March 2024; Accepted 25 March 2024

pathophysiological factors that lead to IDD remain incompletely understood. Notably, individuals afflicted with iron overload conditions, such as thalassemia, sickle cell anemia, and hemochromatosis demonstrate an elevated incidence of intervertebral disc degeneration [3–6]. Previous research conducted by our team has revealed that iron overload constitutes a significant risk factor for IDD. Iron overload may promote IDD by inducing oxidative stress and ferroptosis in cartilage endplate chondrocytes [7]. Nevertheless, the regulatory mechanism governing iron homeostasis remain largely unknown.

Iron, a prominent trace element within the human body, plays a central role in orchestrating a multitude of physiological and biological processes. However, an excess of iron catalyzes the generation of reactive oxygen species (ROS), initiating structural and functional impairment in mitochondria, oxidative stress, lipid peroxidation, and DNA damage. This cascade ultimately leads to ferroptosis [8]. Therefore, iron homeostasis is precisely regulated. Cellular iron homeostasis is mainly regulated by regulating iron influx [9]. The Fe^{3+} in the blood forms a complex with transferrin receptor-1 (TfR1), facilitating its cellular internalization into the cell body. TfR1, ubiquitously expressed in various tissues and organs, assumes a pivotal role in mediating intracellular iron influx and preserving cellular iron homeostasis [10]. Recent studies have highlighted increased TfR1 expression in iron overload conditions like thalassemia, suggesting its role in cellular iron overload and ferroptosis [11]. Elevated TfR1 expression is associated with increased cellular iron levels, Thereby TfR1 is considered an important target for the treatment of central nervous system diseases and tumors [12]. Previous research has shown the upregulation of TfR1 in ferroptosis sensitive cells and the subsequent reduction of ferroptosis through TfR1 downregulation using shRNA [13]. Furthermore, recent studies have also demonstrated that silencing TfR1 can enhance the mitophagy process, suppressing the excessive production of ROS and lipid peroxidation induced by iron overload [14]. These findings suggest that TfR1 not only regulates cellular iron homeostasis and ferroptosis, but also plays a role in a network of interconnected feedback loops. Consequently, TfR1 emerges as a potential target for addressing imbalances in iron metabolism and associated disorders. Regrettably, the role of TfR1 in the context of IDD development remains unexplored.

The intervertebral disc, the body's largest avascular structure in the human body, consists of three distinct components: the central gelatinous nucleus pulposus (NP), the outer annulus fibrosus (AF), and the cartilage endplate (CEP) [15]. The CEP anchors both ends of the vertebral body, CEP chondritis and calcification significantly hinder the oxygen and nutrient supply to the intervertebral disc, initiating and exacerbating IDD [16]. Our previous research has demonstrated that iron overload plays a central role in the progression of IDD by inducing CEP degeneration and calcification, consequently driving IDD. Notably, inhibiting iron overload or ferroptosis could inhibit the IDD progression [7,17]. Furthermore, with aging, the CEP's degeneration intensifies, resulting in a progressively hypoxic microenvironment [18]. Hypoxia, in turn, affects cellular iron metabolism, leading to increased iron flux [19]. It is theorized that heightened iron uptake may enhance mitochondrial energy metabolism and is essential for cell survival in hypoxic environments [20], neverthless, the comprehensive regulatory framework governing cellular iron metabolism in hypoxic settings remains partially elucidated.

In this study, we analyzed the expression pattern of TfR1 in CEP chondrocytes, and explored its role in IDD pathogenesis. Furthermore, we investigated the underlying mechanism of TfR1 mediated iron overload in cartilage endplate osteochondritis and calcification. Additionally, we aimed to investigate the regulatory mechanism of TfR1 expression and determined whether HIF-2α is involved in CEP chondrocytes TfR1 expression and iron metabolism regulation.

2. Materials and methods

2.1. Reagents

The following reagents were used: Tert-butyl hydroperoxide (TBHP, #416665, Sigma–Aldrich, USA), Recombinant Mouse TNF-alpha (TNF-α, 410-MT-010, R&D, USA), Ferristain II (#C1144, Sigma–Aldrich, USA), Ferric ammonium citrate (FAC, #F5879, Sigma–Aldrich, USA), Ethidium bromide (EthBr, #S3689, Selleck, USA).

2.2. Cell isolation and culture

Cartilage endplate (CEP) chondrocytes were isolated from the endplates of 1-week-old C57BL/6J male mice and subsequently cultured for 1 or 2 passages following established protocols. To begin, the mice were humanely euthanized via cervical dislocation and subjected to aseptic sterilization through immersion in 75% ethyl alcohol for 20 min. Subsequently, under microscopic guidance (Leica, Germany), the paravertebral muscle and ligament were meticulously removed, and the cartilage endplates were dissected. These dissected samples were subjected to a sequential enzymatic digestion process, involving exposure to 0.25% EDTA trypsin (Gibco, USA) for 30 min and 0.25% solution of type II collagenase (Sigma–Aldrich, USA) for 6h at 37 °C. Following flushing and centrifuging with phosphate-buffered saline (PBS, Gibco, USA), the primary CEP chondrocytes were resuspended and cultured in Dulbecco's modified Eagle medium/Ham's F-12 (DMEM/F12, Gibco, USA) supplemented with 10% fetal bovine serum (FBS, Gibco, USA) and 1% penicillin-streptomycin (P/S, Gibco, USA) at 37 °C under 5% CO2. After 24h, the medium was changed and the adherent cells were passaged once they attained 80–90% confluence.

2.3. Western blot analysis

CEP chondrocytes were seeded into 6-well plates at a density of 5×10^5 cells/well. Subsequent protein extraction was carried out using RIPA lysis buffer (#CW2333, CWBIO, Beijing, China) supplemented with 1% proteinase inhibitor cocktail (#HY-K0010, MCE, USA) and 1% phosphatase inhibitor cocktail (#CW2383, CWBIO, Beijing, China) after CEP chondrocytes were washed by ice-cold PBS for 3 times as previously reported. Briefly, the extract was transferred to a centrifuge tube for 30 min of lysing on ice and then centrifuged at 12000r/min and for 15 min at 4 °C. The resulting supernatant was collected for quantification of protein concentration using a BCA assay kit (#PC0020, Solarbio, Beijing, China). Post denaturation through heating at 100 °C for 10 min in loading buffer (#P0015L, Beyotime, Shanghai, China) denaturation, equal quality of proteins (25 μg) were loaded onto 10% sodium dodecyl sulfate-polyacrylamide gel electrophoresis (SDS-PAGE) and transferred to 0.2 μm methanol-activated PVDF membrane (#ISEQ00010, Millipore, USA. Following 1h of incubation with 5% skim milk diluted in tris-buffered saline Tween 20 (TBST) at room temperature, the membranes were probed with appropriate primary antibodies overnight at 4 °C. Subsequently, after another 1h of incubation with HRP Conjugated Goat Anti-rabbit/mouse secondary antibodies (#BA1056, Boster, Wuhan, China, dilution 1:5000) at room temperature, protein bands were visualized using Immobilon Western HRP substrate Kit (#WBKLS0100 , Millipore, USA) and analyzed with BandScan scanner (Millipore, USA). Band density was quantified using image J version 2.90 and GAPDH was served as internal control to normalize the results. The primary antibodies used were as follows: TfR1 (#ab84036, Abcam, dilution 1:1000), HIF-2α(#BM3997, Boster, dilution 1:1000), IRF3(#4302, Cell Signaling Technology, dilution 1:1000), p-IRF3(Ser396, #29047, Cell Signaling Technology, dilution 1:1000), BNIP3(#3769S, Cell Signaling Technology, dilution 1:1000), GPX4 (#ab125066, Abcam, dilution 1:5000), SLC7A11 (#26864-1-AP, Proteintech, dilution 1:1000), cGAS (#A8335, ABclonal, dilution 1:1000), STING (#19851-1-AP, Proteintech, dilution 1:1000), DRP1 (#12957-1-AP, Proteintech, dilution 1:1000), MFF

(#17090-1-AP, Proteintech, dilution 1:1000), FIS1(#10956-1-AP, Proteintech, dilution 1:1000), MMP3(#BM4074, Boster, dilution 1:1000), MMP13(#18165-1-AP, Proteintech, dilution 1:1000), COL2 (#28459-1-AP, Proteintech, dilution 1:1000), SOX9 (#A00177-2, Boster, dilution 1:1000), COL10 (#BA2023, Boster, dilution 1:1000), RUNX2 (#PB0171, Boster, dilution 1:1000), GAPDH (#10491-1-AP, Proteintech, dilution 1:5000).

2.4. Immunofluorescence analysis

First, CEP chondrocytes were seeded in Circle Microsope Cover Glasses at a density of 1×10^4/well. Subsequent to aspirating the culture medium., the treated cells underwent fixation using 4% paraformaldehyde (#G1101, Servicebio, Wuhan, China) for 30 min at room temperature. Following fixation, the cells were subjected to permeabilization utilizing 0.1% Triton X-100 (#T8200, Solarbio, Beijing, China) for 10 min and then blocked with PBS containing 5% bovine serum albumin (BSA, #BS114, Biosharp, Beijing, China) for 1 h at 37 °C. Thereafter, the cells were incubated with primary antibodies at 4 °C overnight, followed by treatment with Cy3-conjugated goat anti-rabbit secondary antibody (#A0516, Beyotime, Shanghai, China, dilution 1:500) in the darkness at room temperature for 1 h. Finally, nuclei were counterstained with 4,6-diamidino-2-phenylindole (DAPI, #C0065，Solarbio, Beijing, China) for 10 min. Notably, the cells need rinse thrice with PBS for 5 min each before fixation, permeabilization, blocking, incubation with primary and secondary antibody procedure. Fluorescence microscope (Olympus, Japan) was used to analyze the fluorescence intensity of COL2 (#28459-1-AP, Proteintech, dilution 1:500), GPX4 (#67763-1-lg, Proteintech, dilution 1:200), DRP1 (#12957-1-AP, Proteintech, dilution 1:500) and FIS1(#10956-1-AP, Proteintech, dilution 1:500).

2.5. Mito-tracker red co-localization staining with LC3B/BNIP3/DRP1/FIS1

Before the same procedures of fixation, permeabilization, blocking and nuclei staining conducted as previously described, the treated live CEP chondrocytes were marked with MitoTracker™ Red CMXRos probes (#M7512, ThermoFisher, USA, dilution 1:5000) in the dark at 37 °C for 20 min. Following incubation with primary antibodies against BNIP3(#3769S, Cell Signaling Technology, dilution 1:200), LC3B (#ab192890, abcam, dilution 1:200), BNIP3(#3769S, Cell Signaling Technology, dilution 1:300) and FIS1(#10956-1-AP, Proteintech, dilution 1:300) at 4 °C overnight, the cells were then treated with FITC-conjugated goat anti-rabbit secondary antibody (#A0562, Beyotime, Shanghai, China 1:500) in the dark at 37 °C for 1.5 h. The co-localizations of BNIP3, LC3B, DRP1, FIS1 and mitochondria were imaged with a positive fluorescence microscope (BX6; Olympus, Japan), respectively.

2.6. Intracellular reactive oxygen species (ROS) assay

For the assessment of intracellular ROS level, the fluorescent probe, dichloro-dihydro-fluorescein diacetate (DCFH-DA, #S0033, Beyotime, Shanghai, China), was employed, following the manufacturer's instruction. Briefly, after incubation with the DCFH-DA probe mixture (10uM) in serum-free DMEM/F12 medium for 20 min in the dark and changing serum-free medium, images were acquired under an inverted fluorescence microscopy (Axio Observer A1; Carl Zeiss, Germany).

To facilitate a quantitative assessment of ROS level *in vitro*, flow cytometry (FCM) was subsequently employed. In alignment with the aforementioned protocol for the ROS assay kit, CEP chondrocytes were collected to calculate the mean fluorescence intensity, using an LSRFortessa FCM (BD Biosciences, Franklin Lakes, NJ，USA).

2.7. Mitochondrial membrane potential (MMP, ΔΨM)

ΔΨM changes were evaluated via mitochondrial membrane potential kit (#C2006, Beyotime, Shanghai, China). Briefly, after incubation with the JC-1 staining working solution for 20 min at 37 °C, CEP chondrocytes were rinsed with ice-cold JC-1 washing buffer for 3 times. Multimeric JC-1 with high red fluorescence shifts to monomeric JC-1 with high green fluorescence, suggesting the loss of ΔΨM. The ΔΨM changes were captured by an inverted fluorescence microscope (Axio Observer A1; Carl Zeiss, Germany).

2.8. Mitochondrial specific fluorescence staining

Mito-tracker staining was performed to visualize mitochondria, in accordance with the protocol of the Mito-tracker Green assay kit (#C1048 ，Beyotime, Shanghai, China). Mitochondrial morphology was observed using an inverted fluorescence microscopy (Axio Observer A1; Carl Zeiss, Germany).

2.9. PicoGreen and mito-tracker red co-staining

For mtDNA staining, the CEP chondrocytes were stained with MitoTracker™ Red CMXRos probes (#M7512, ThermoFisher, USA, dilution 1:5000) for 20 min, followed 20 min of incubation in PicoGreen dsDNA Quantitation Reagent (#12641 ES, Yeasen, Shanghai, China, dilution 1:500) at 37 °C after washed with PBS. Then, the microsope cover glasses were observed and imaged using a confocal fluorescence microscope (TCS SP8; Leica Microsystems, Biberach, Germany).

2.10. Measurement of labile iron levels

The intracellular pool of iron ions can be monitored by the quenching of fluorescence of Phen Green™ FL (#P6763, ThermoFisher, USA). The emission intensity of the Phen Green FL indicator is contigent on the concentration of iron ions. Briefly, after loading with Phen Green™ FL (0.5uM) for 30 min at 37 °C, the fluorescence intensity was observed under an inverted fluorescence microscopy (Axio Observer A1; Carl Zeiss, Germany). This was conducted every 5min–10min over 6 intervals during an incubation period with 100uM ferric ammonium citrate.

For further investigation of intracellular Fe^{2+} levels, the treated CEP chondrocytes were washed 3 times in serum-free medium and perfused with 1uM FerroOrange (#F374, Dojindo, Kumamoto, Japan) for 30 min at 37 °C. After that, images were immediately obtained with an inverted fluorescence microscopy (Axio Observer A1; Carl Zeiss, Germany).

2.11. Animal grouping and treatment

A total of 24 male C57BL/6 mice (8 weeks old) were randomly assigned to 3 groups (n = 8 per group): control group, IDD group and IDD + Ferristain II group (10 mg/kg/2d). The surgically-induced IDD model was established as detailed in prior protocols [21]. In brief, after obtaining the mice's weights and administering anesthesia, the surgical procedure involved exposing the L4/5 level, which was confirmed by counting the lumbar vertebrae in a preliminary radiograph. Subsequently, bilateral facet joints at the L4/5 level, supra- and interspinous ligaments were transected. Mice in IDD group were administered an equal amount of saline intraperitoneally every other day for 12 weeks until euthanasia.

In a subsequent animal experiment, 18 male C57BL/6 mice (8 weeks old) were utilized. These mice were sacrificed at intervals of 1, 2 and 3 months (n = 6 per group) following the identical IDD procedure. Additionally, in the third animal experiment, a group of mice aged 1,3,6 and 16 months (n = 6 per group) respectively, without undergoing surgery, were sacrificed. Corresponding spinal tissues were harvested for micro-CT and immunohistochemistry assessment. All animal experiments were approved by the Animal Care Committee of Shandong

Provincial Hospital affiliated to Shandong First Medical University.

2.12. Micro-CT analysis

The excised spine specimens, devoid of muscles, were fixed in 4% paraformaldehyde (PFA) for 24 h. To assess alterations in the micro-architecture of the surgically modeled segment, micro-CT (Scanco Viva-CT80, Scanco Medical AG, Basserdorf, Switzerland) was then used to determine morphometric indices, such as intervertebral disc height and percent bone volume (BV/TV), from the volume of interest (VOI), with the resolution of 11.6 μm, 70 kVp, and 114 μA. And the three-dimensional (3D) images of the CEP were collected by built-in software.

2.13. Histology and immunohistochemical assay

Lumbar tissues were subsequently decalcified (EDTA buffer, 0.5M, pH7.2), embedded, sectioned and stained with hematoxylin-eosin (H&E), performed to observe the morphology of cartilage and subchondral bone, as previously mentioned [7]. The severity of IDD was evaluated by lumbar intervertebral disc degeneration assessment scoring system.

For immunohistochemistry (IHC) staining, as previously described, after deparaffinization, rehydration,blocking, and antigen retrieval, the sections (4 μm, coronal plane) were then incubated with primary antibodies against COL2 (#GB11021, Servicebio, dilution 1:400), MMP3 (#BM4074, Boster, dilution 1:500), STING (#19851-1-AP, Proteintech, dilution 1:50), TfR1 (#ab84036, Abcam, dilution 1:50) and HIF-2α (#GB11864, Servicebio, dilution 1:100) overnight at 4 °C. Next, the sections were stained with the HRP-conjugated secondary antibody (#GB23303, Servicebio, dilution 1:200) for 30 min at room temperature followed colored with DAB and counterstained with hematoxylin. Immune positive staining of 5 CEP fields randomly selected was quantitatively analyzed using Image Pro Plus software.

2.14. siRNA transfection

To induce the knockdown of HIF-2α, STING and TfR1 in mice CEP chondrocytes, transfection procedures were carried out utilizing specific siRNAs. The siRNA employed were HIF-2α-siRNA (siHIF-2α), STING-siRNA (siSTING) and TfR1-siRNA (siTFR1). These transfections were performed using the riboFECTTMCP kit (Ribo Bio, Ribobio Co. Ltd., Guangzhou, China). The CEP chondrocytes were transitorily transfected with 100 nM of each siRNA for 48h according to the manufacturer's instructions. After transfection, silence efficiency was verified by western blot and the most effective siHIF-2αand siTfR1 were screened for subsequent analysis.

2.15. Induction of osteogenic differentiation and alizarin red staining

CEP chondrocytes were seeded in 12-well plates at a density of 1×10^5 cells/ml and the α-MEM medium containing 10% FBS, 1% P/S, 1% L-glutamine,10-7M dexamethasone, 10 mM β-glycerophosphate and 50ug/ml ascorbic acid, were added when the cell density reached 70% confluence. After induction for 3 weeks , mineralized nodules *in vitro* were fixed with 4% paraformaldehyde for 30 min and stained with alizarin red (#G1038, Servicebio, Wuhan, China) for 15 min. Then the degree of mineralization was quantitatively assessed by spectrophotometry. Specially, the red dye was dissolved by 10% (wt/vol) cetylpyridinium chloride (Sigma–Aldrich, St. Louis, MO) and calculated optical density at 570 nm.

2.16. Evaluation of apoptosis by annexin V-FITC/PI staining

The treated adherent CEP chondrocytes were collected and stained with annexin V-FITC/PI (MA0220, Meilunbio, Dalian, China) for 20 min at room temperature in the dark and then detected by BD LSRFortessa flow cytometer (BD Biosciences, Franklin Lakes, NJ , USA). The apoptotic cells labeled with annexin V+/PI- and V+/PI+ were screened respectively.

2.17. Statistical analysis

The data are presented as the mean ± standard deviation (SD). The figure legends provide information regarding the number of experimental replicates and the level of significance. GraphPad Prism software version 8.0 was employed for both generating graphical representations and conducting statistical analyses. For comparisons between two groups, Student's t-test was utilized. In scenarios involving multiple groups, one-way analysis of variance (ANOVA) was applied to ascertain significant differences. The P value was indicated by stars: n. s. no significance, *P < 0.05, **P < 0.01, ***P < 0.001.

3. Results

1. IDD pathogenic environment disrupted iron homeostasis and promoted iron influx via promoting TfR1 expression

To unravel the potential relationship between the expression of TfR1 and IDD pathogenesis, we started with an exploration of TfR1 expression in two distinct IDD models. Given that aging is the primary trigger for IDD, we first examined the expression pattern of TfR1 in aging mice. As shown in Fig. 1A and B, the TfR1 positive chondrocytes in the CEP increased with aging, with the highest propotion observed in 16-month-old mice. To better understand the complex mechanisms involved in IDD, we then investigated the role of mechanical stress, a significant independent risk factor. To simulate the consequences of unbalanced mechanical loading, we executed Lumbar Spine Instability (LSI) surgery on 1-month-old male mice, thereby inducing the IDD model. As shown in Fig. 1C and D, the CEP undergoes degeneration and ossification at 1 month after surgery characterized by the presence of substantial bone tissue and vacated chondrocyte lacuna. Strikingly, immunostaining analysis showed that the number of cells positive for TfR1 significantly increased in degenerated CEP after 1 and 2 months after LSI surgery compared to the control group. Intrigued by these findings, we sought to ascertain the impact of IDD related environmental factors on TfR1 expression. Therefore, we exposed isolated CEP chondrocytes to conditions replicating the pathogenic environment of IDD through TBHP and TNF-α treatment. As shown in Fig. 1E and I, the protein expression of TfR1 was upregulated in CEP chondrocytes by the TBHP and TNF-α treatment. Complementary immunofluorescence staining substantiated this augmented TfR1 expression in chondrocytes treated with TBHP (Fig. 1F). Along with the elevated protein expression of TfR1, the iron influx increased after TBHP and TNF-α treatment, as indicated with significant higher ferrous ions in CEP chondrocytes of TBHP and TNF-α treatment group (Fig. 1G and J). Ferroptosis is a newly identified iron dependent programmed cell death. Elevated cellular ferrous ions content would increase the sensitivity to ferroptosis. Our results also showed that TBHP promoted CEP chondrocytes ferroptosis with decreased ferroptosis markers, GPX4 and SLC7A11 when TBHP concentration reached over 10 μM (Fig. 1H). In conclusion, these results suggest a positive correlation between TfR1 expression and IDD progression. IDD pathogenic environment could disrupt iron homeostasis and promote iron influx via regulating TfR1 expression.

2. TfR1 knockdown restored oxidative stress and TNF-α induced CEP degeneration

To further determine the role of TfR1 in CEP degeneration, TfR1 siRNA was synthesized and transfected into CEP chondrocytes, and CEP chondrocytes were treated with TBHP and TNF-α to induce chondrocytes extracellular matrix (ECM) degradation and osteogenic differentiation. As shown in Fig. 2A, compared with TBHP and TNF-α

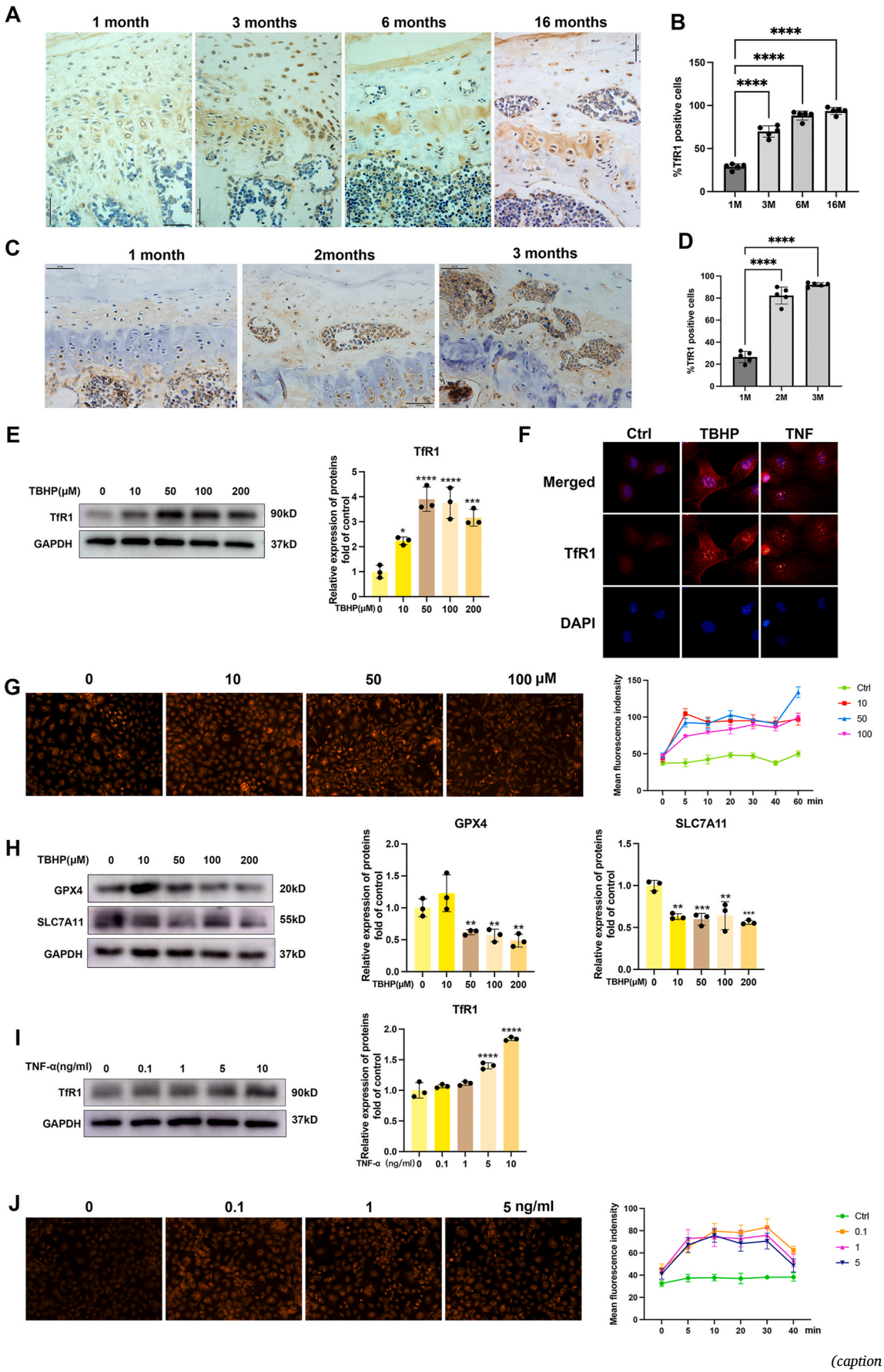

(caption on next page)

Fig. 1. IDD pathogenic environment disrupted iron homeostasis and promoted iron influx via promoting TfR1 expression. A Representative images of IHC of TfR1 in CEP from 1-month aged, 3-month aged, 6-month-aged and 16-month-aged mice. B Quantitative analysis of TfR1-positive chondrocytes as a proportion of the total chondrocytes. C Representative images of IHC of TfR1 in CEP from mice after 1month, 2 months and 3 months after LSI surgery (n = 5, scale bar = 50 μm). D Quantitative analysis of TfR1-positive chondrocytes as a proportion of the total chondrocytes. E Representative western blotting images of TfR1 and semi-quantitative analysis of band density in TBHP treated CEP chondrocytes. F Representative immunofluorescence images of TfR1 in CEP chondrocytes treated with TBHP and TNF-α. G Representative images of ferrous ions in CEP chondrocytes after TBHP treatment for 60 min. Iron influx was quantified and recorded at 5-10-20-30-40-60 min. H Representative western blotting images of GPX4, SLC7A11 and semi-quantitative analysis of band density in TBHP treated CEP chondrocytes. I Representative western blotting images of TfR1 and semi-quantitative analysis of band density in TNF-α treated CEP chondrocytes. J Representative images of ferrous ions in CEP chondrocytes after TNF-α treatment for 60 min. Iron influx was quantified and recorded at 5-10-20-30-40-60 min. Data are shown as the mean ± SD of at least three independent experiments. The P value is indicated by stars: *P < 0.05, **P < 0.01, ***P < 0.001, ****P < 0.0001.

treatment group, knockdown of TfR1 significantly reversed the inhibition of type II collagen synthesis, as shown by increased red fluorescence intensity. The western blot results showed that TfR1 knockdown also promoted the SOX9 proteins expression, inhibited the ECM degradation enzymes, MMP3 and MMP13 expression (Fig. 2B-C, J-K). Given the established association between oxidative stress and CEP chondrocyte osteogenic differentiation, we proceeded to explore whether TfR1 knockdown could potentially counteract TBHP induced osteogenic differentiation and calcification. As shown in Fig. 2D-G, TfR1 siRNA transfection significantly inhibited TBHP induced COL10 and RUNX2 expression. The alizarin red staining results also showed that TfR1 siRNA transfection inhibited the calcium nodules formation. Lastly, we investigated whether TfR1 knockdown could inhibited oxidative stress induced apoptosis. As shown in Fig. 2H-I, Annexin V-FITC/PI flow cytometric analysis showed that the oxidative stress-induced early apoptosis, late apoptosis and necrosis in chondrocytes significantly decreased after TfR1 knockdown. These findings suggest that TfR1 contributes to CEP degeneration and calcification, and TfR1 knockdown could restore oxidative stress and TNF-α induced CEP degeneration.

3. TfR1 inhibitor ameliorated CEP calcification and IDD development

Based on above findings, we applied Ferstatin II to further illustrate the therapeutic effects of targeting TfR1 on IDD progression. Ferstatin II, a novel and selective TfR1 inhibitor that can substantially suppress TfR1 activity [22]. Mice were intraperitoneal injected with Fer-II once a week after lumbar spine instability (LSI) surgery. The IHC results exhibited less TfR1 positive chondrocytes in CEP of LSI mice injected with Fer-II compared with LSI mice, indicating Fer-II successfully inhibited TfR1 expression *in vivo* (Fig. 3C). The HE results showed that Fer-II administration significantly inhibited IDD progression with lower histological score of discs. Compared to IDD group, the nucleus pulposus of mice in Fer-II group contained abundant notochordal cells surrounded by large zones of extracellular matrix, and the cartilage endplates were hyaline cartilages composed of chondrocytes (Fig. 3A and B). Consistently, increased protein levels of MMP3 (Fig. 3D) and reduced expression of COL2 (Fig. 3E) in cartilage of IDD mice, were greatly repressed by Fer-II treatment. In addition, the CEP calcification was examined by micro-CT analysis. As shown in Fig. 3F and G, Fer-II administration significantly inhibited the CEP calcification with decreased bone mineral density of CEP. Together, these data demonstrates that the administration of Fer-II could attenuate IDD development and CEP calcification by inhibiting TfR1.

4. TfR1 mediated iron influx contributes to CEP chondrocytes mitochondrial destruction and ferroptosis

Given that our previous finding that iron overload could lead to CEP chondrocytes oxidative stress and ferroptosis, and the essential role of mitochondrial in ferroptosis and IDD [23], we further explored the functional role of TfR1 in mitochondria function and ferroptosis. Firstly, the iron influx was examined after TfR1 knockdown. As shown in Fig. 4A, TfR1 knockdown significantly reduced iron influx and lowered the concentration of cellular ferrous ions. Healthy chondrocytes typically display a wire-like shape. However, when treated with TBHP, the normal morphology of mitochondria is disrupted, resulting in a significant increase in the number of shortened or granulated mitochondria. TfR1 knockdown was able to restore the normal mitochondrial morphology of chondrocytes (Fig. 4B). Interestingly, we also found that TfR1 knockdown inhibited oxidative stress induced mitochondrial fission process with decreased Drp1, MFF and FIS1 proteins expression and promoted the BNIP3 mediated mitophagy process (Fig. 4C). Similar results were obtained by the immunofluorescence analysis. TfR1 knockdown promoted the colocalization green immunofluorescence stained BNIP3 protein and red immunofluorescence stained mitochondria (Fig. 4E). Also TFR1 knockdown inhibited the expression of FIS1 protein expression and localization in mitochondria, these results indicated the activation of mitophagy process and inhibition of mitochondrial destruction (Fig. 4D). We next investigated whether reducing iron influx through TfR1 silencing could inhibit the CEP chondrocytes ferroptosis. As shown in Fig. 4F and G, TfR1 knockdown significantly inhibited TBHP and FAC (800 μM) induced ferroptosis with decreased GPX4 and SLC7A11 proteins expression. In summary, our findings highlight the intricate network linking TfR1, iron influx, mitochondrial function, and ferroptosis in the context of CEP chondrocytes. This complex interplay underscores the potential significance of targeting TfR1 as a therapeutic avenue in managing mitochondrial-driven ferroptosis in IDD.

5. Mitochondrial mtDNA release and c-GAS/STING activation participates in iron overload induced CEP chondrocytes degeneration

We next investigated the underlying mechanisms of CEP degeneration induced by iron overload. Mitochondria are the main organism of cellular iron metabolism and mitochondrial dysfunction plays an important role in IDD progression [24]. CEP chondrocytes were treated with increasing concentrations of FAC and we found that FAC significantly promoted the mitochondrial destruction with elevated mitochondrial fission proteins, such as Drp1, MFF and FIS1(Fig. 5A). To further examine the effect of iron overload in mitochondrial destruction, immunofluorescence staining was then performed to examine the mitochondrial morphology and colocalization of Drp1 and mitochondria. As shown in Fig. 5B, FAC treatment (100 μm) significantly increased the colocalization of green immunofluorescence stained Drp1 and red mitochondria, also much more granulated mitochondria were observed in FAC treatment group. Simultaneously, our investigation unveiled the release of mitochondrial mtDNA into the cytoplasm, further accentuating the impact of iron overload. As shown in Fig. 5E, the green immunofluorescence stained dsDNA probe in the cytoplasm increased after the TBHP and TNF-α treatment, indicating that oxidative stress and proinflammatory cytokines promoted the mtDNA leakage from the mitochondria. Western blot analysis also demonstrated that FAC and TBHP promoted the stimulator of interferon genes (STING) protein expression and its downstream effector p-IRF3 in a dose dependent manner (Fig. 5C and D). The immunohistochemistry analysis also indicated a significant increase in STING protein expression in aged mice and mice with lumbar spine instability (LSI) surgery (Fig. 5G and H). Intriguingly, STING knockdown emerged as a potent countermeasure against iron overload induced CEP chondrocyte degeneration, STING silencing resulted in decreased ECM degradation enzymes, MMP3 and

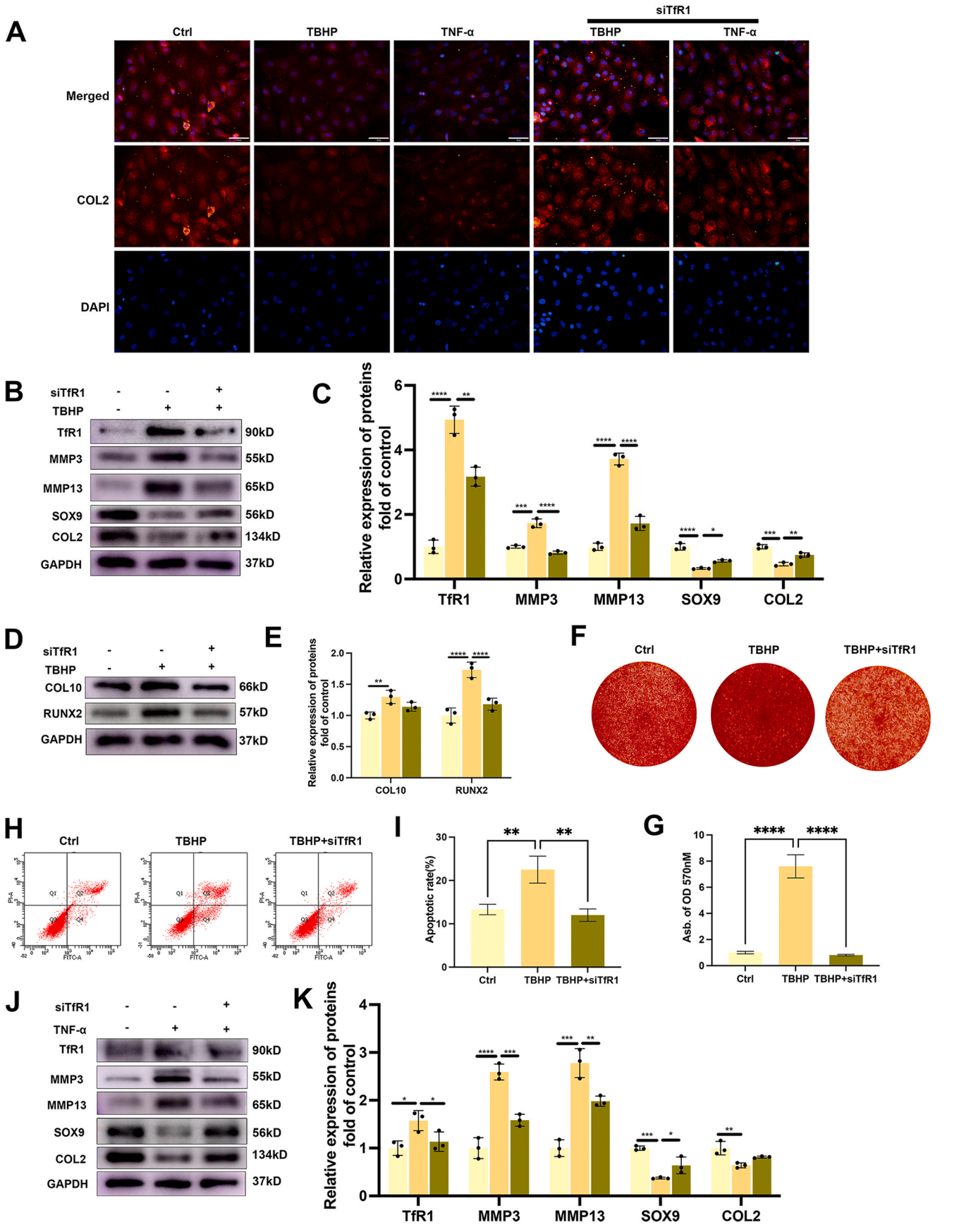

(caption on next page)

Fig. 2. TfR1 knockdown restored oxidative stress and TNF-α induced CEP degeneration. A Representative immunofluorescence images of COL2 in TBHP and TNF-α treated CEP chondrocytes with or without TfR1 siRNA transfection. Scale bar = 50 μm. B–C Representative western blotting images of TfR1, MMP3, MMP13, SOX9, COL2 and semi-quantitative analysis of band density in TBHP treated CEP chondrocytes. D-E Representative western blotting images of COL10, RUNX2 and semi-quantitative analysis of band density in TBHP treated CEP chondrocytes. F Alizarin Red staining for calcium deposition in endplate chondrocytes. G Semi-quantitative analysis of the mineralized nodule in endplate chondrocytes. H–I Annexin V-FITC/PI flow cytometric analysis was conducted to evaluate apoptosis rate induced by TBHP and TfR1 siRNA transfection. J-K Representative western blotting images of TfR1, MMP3, MMP13, SOX9, COL2 and semi-quantitative analysis of band density in TNF-α treated CEP chondrocytes. Data are shown as the mean ± SD of at least three independent experiments. The P value is indicated by stars: *P < 0.05, **P < 0.01, ***P < 0.001, ****P < 0.0001. (For interpretation of the references to colour in this figure legend, the reader is referred to the Web version of this article.)

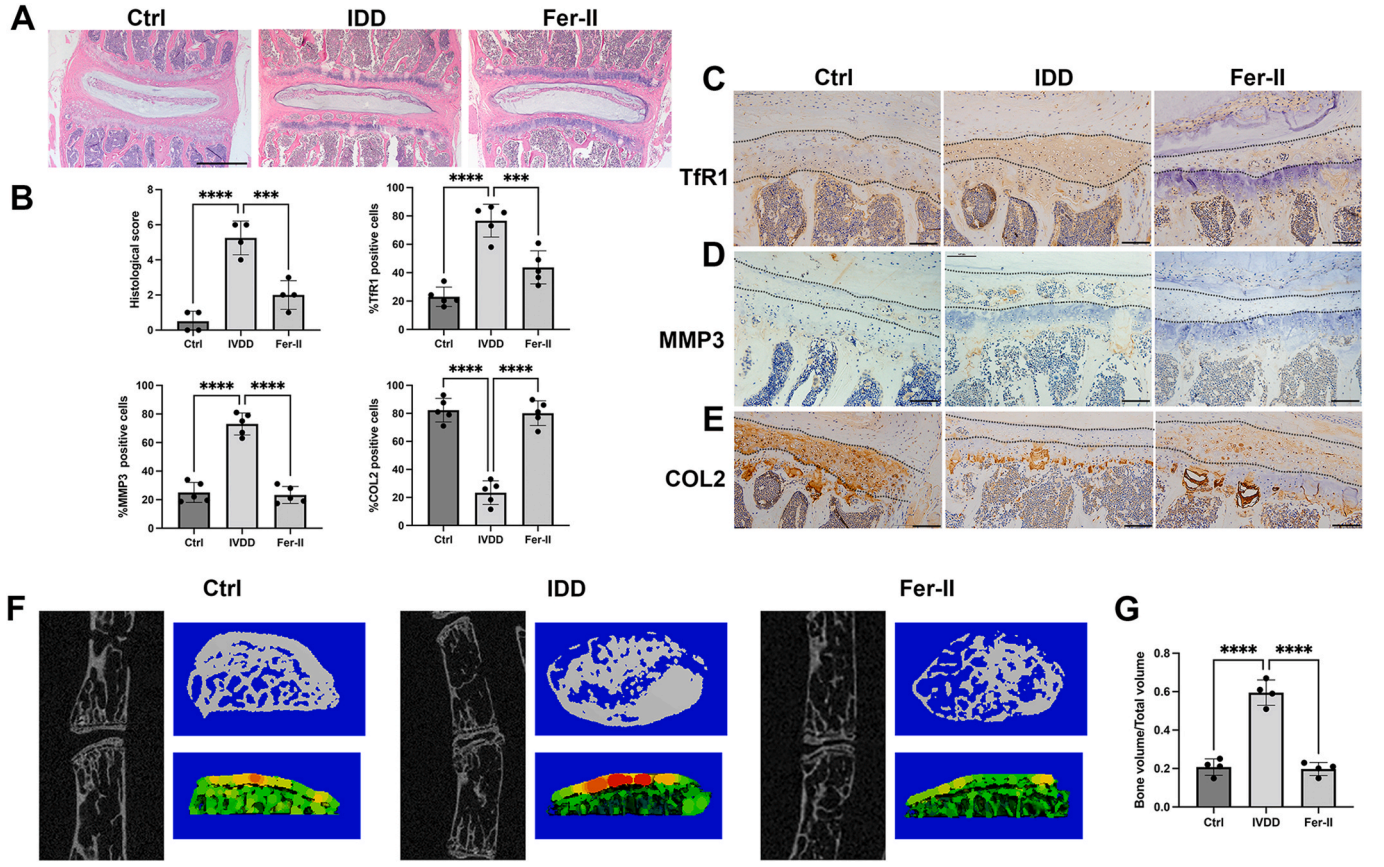

Fig. 3. TfR1 inhibitor ameliorated CEP calcification and IDD development. A Eight-week aged mice were randomly divided in three groups and intra-peritoneally injected Feristatin II solution followed by LSI surgery. HE staining of L4/5 intervertebral discs in the Ctrl group, IDD group, and Fer-II group. scale bar = 200 μM. B Histological score of the L4–5 segments of the lumbar spine among the three groups and the ratio of positive cells for TFR1, SOX9, MMP3 from each group. C-E Immunohistochemistry for TfR1, MMP3, SOX9 in the Ctrl, IDD, and Fer-II groups. Scale bar = 100 μm. F Micro-CT analysis, 3D reconstruction, and X-ray images of cartilage endplate. G Quantification of cartilage endplate calcification via microarchitecture parameters [bone volume per tissue volume (BV/TV)]. Data are shown as the mean ± SD. N = 5, The P value is indicated by stars: ***P < 0.001, ****P < 0.0001.

MMP13, coupled with increased type II collagen expression (Fig. 5F). These results indicated that mitochondrial mtDNA release and c-GAS/STING activation participates in iron overload induced CEP chondrocytes degeneration.

6. TfR1 mediated mtDNA release play essential roles in the cGAS-STING activation and CEP chondrocytes degeneration

mtDNA has been demonstrated to be an important damage associated molecular pattern molecules (DAMPs), which could be recognized by cGAS-STING pathway [25]. As shown in Fig. 6A and B, TfR1 inhibition reversed the activation of cGAS-STING pathway and inhibited the decrease of mitochondrial membrane potential. Also our results found that TfR1 knockdown inhibited TBHP and TNF-α induced mtDNA release with decreased green immunofluorescence stained dsDNA in the cytoplasm. To determine whether mtDNA served as a DAMP to stimulate STING activation in response to TBHP, CEP chondrocytes were depleted of mtDNA via pretreatment of ethidium bromide (EtBr) to inhibit mtDNA replication. After confirming by confocal microscopy that ethidium-bromide-treated cells were depleted of mtDNA (Fig. 6E), western blot results showed that TBHP induced cGAS-STING activation was inhibited. Moreover, EthBr inhibited TBHP induced ECM degradation with increased SOX9 and COL2 expression, and decreased matrix enzymes MMP3 and MMP13 expression. These results indicated that TfR1 mediated mtDNA release play essential roles in the cGAS-STING activation and CEP chondrocytes degeneration.

7. TfR1 was upregulated in a HIF-2α dependent manner

Research has shown that hypoxia could affect cellular iron metabolism and promote iron flux. Hypoxia-inducible factors (HIFs) play an important role in enabling chondrocytes to adapt to hypoxia environment, maintaining chondrocyte phenotype and regulating energy metabolism [26]. We speculated that the upregulation of TfR1 might be related to the hypoxia-inducible factors. We next examined the expression pattern of HIF-2α of CEP during IDD progression. As shown in

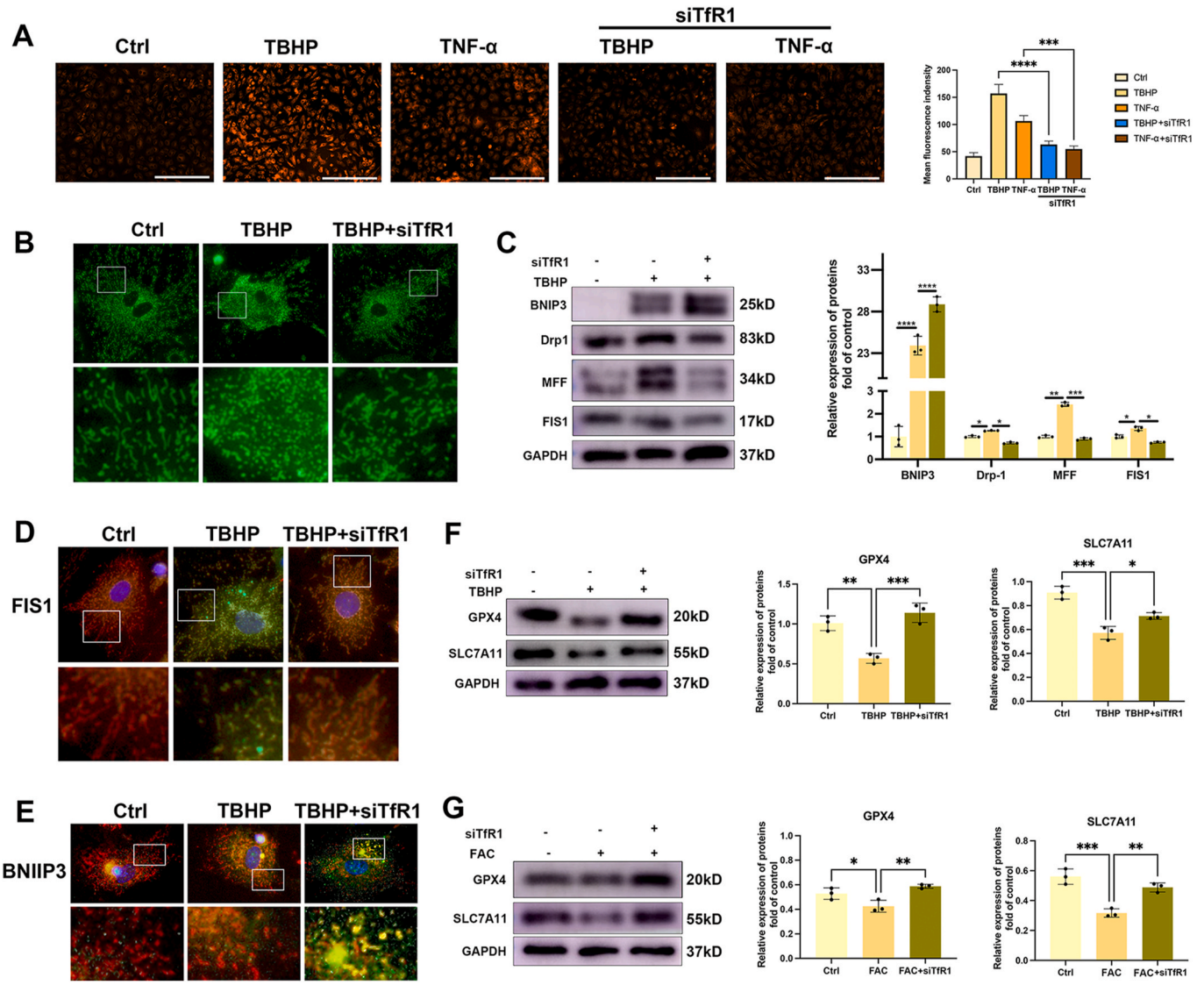

Fig. 4. TfR1 mediated iron influx contributes to CEP chondrocytes mitochondrial destruction and ferroptosis. A Representative staining for ferrous ions in the indicated group and statistical analysis of fluorescence intensity. scale bars = 200 μm. B Representative mitochondrial morphology in TBHP treated CEP chondrocytes with or without TfR1 siRNA transfection using Mito-tracker Green staining. C Representative western blotting images of BNIP3, Drp1, MFF, FIS1 and semi-quantitative analysis of band density in TBHP treated CEP chondrocytes with or without TfR1 siRNA transfection. D-E Representative immunofluorescence images of FIS1 and BNIP3 in TBHP treated CEP chondrocytes with or without TfR1 siRNA transfection. Mitochondria were stained with red mitotracker probe, BNIP3 and Drp1 were stained with green immunofluorescence. F Representative western blotting images of GPX4, SLC7A11 and semi-quantitative analysis of band density in TBHP treated CEP chondrocytes with or without TfR1 siRNA transfection. G Representative western blotting images of GPX4, SLC7A11 and semi-quantitative analysis of band density in 800 μM FAC treated CEP chondrocytes with or without TfR1 siRNA transfection. Data are shown as the mean ± SD of at least three independent experiments. The P value is indicated by stars: *P < 0.05, **P < 0.01, ***P < 0.001, ****P < 0.0001. (For interpretation of the references to colour in this figure legend, the reader is referred to the Web version of this article.)

Fig. 7A and B, the immunohistochemistry analysis also showed that HIF-2α protein expression was significantly elevated in aged mice and mice with lumbar spine instability (LSI) surgery. Also *in vitro* experiments demonstrated that oxidative stress and pro-inflammatory cytokines promoted CEP chondrocytes HIF-2α expression (Fig. 7C and D). To determine whether HIF-2α could directly regulate iron influx, CEP chondrocytes were transfected with HIF-2α siRNA and the levels of ferrous ions were detected using a ferric ion probe. The results showed that ferrous ions level was reduced in HIF-2α knockdown chondrocytes compared to THBP treated chondrocytes (Fig. 7E). Our results showed that the TfR1 proteins expression was inhibited after HIF-2α knockdown (Fig. 7F and G). Furthermore, we also examined the mitochondrial fission proteins expression and the mtDNA in cytoplasm. As shown in Fig. 7H, HIF-2α knockdown also significantly inhibited the mitochondrial destruction and the mtDNA leakage to the cytoplasm. These results indicated that HIF-2α take parts in regulating CEP chondrocytes iron metabolism, and TfR1 is upregulated in a HIF-2α dependent manner during IDD progression.

4. Discussion

The pathogenesis of IDD is very complex, aging, mechanical stress, and metabolic abnormalities could lead to endplate osteochondritis and oxidative stress damage, which are important contributors to endplate degeneration and the occurrence of IDD [27]. Recent studies have demonstrated that the aberrant accumulation of iron in tissues and cells is linked to many diseases, including chronic renal failure, Parkinson's disease, Alzheimer's disease, osteoporosis and Arteriosclerosis [28]. Our

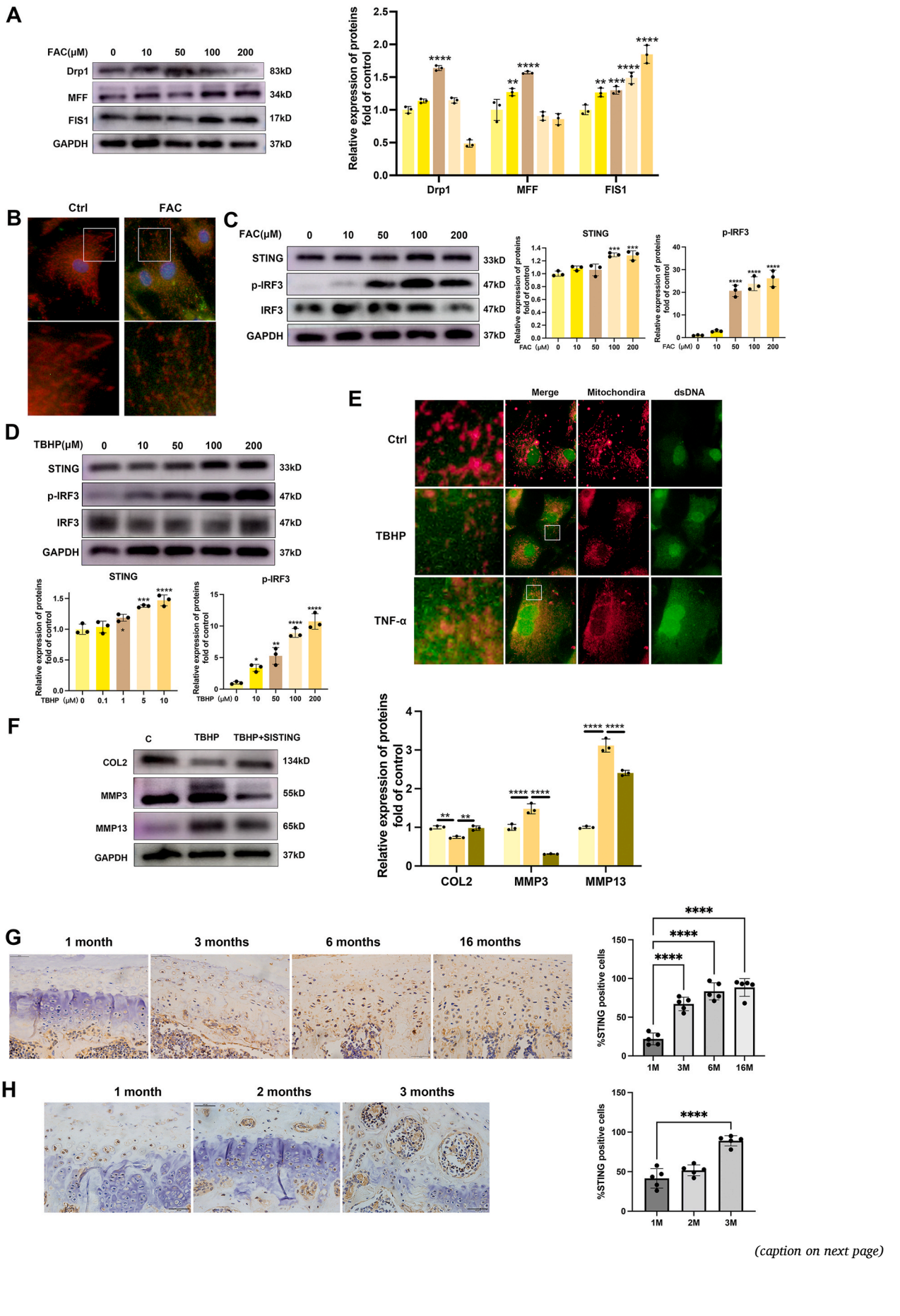

(caption on next page)

Fig. 5. Mitochondrial mtDNA release and c-GAS/STING activation participates in iron overload induced CEP chondrocytes degeneration. A Representative western blotting images of Drp1, MFF, FIS1 and semi-quantitative analysis of band density in FAC treated CEP chondrocytes. B Representative immunofluorescence images of Drp1 in FAC treated CEP chondrocytes. C-D Representative western blotting images of STING, IRF3, p-IRF3 and semi-quantitative analysis of band density in TBHP and FAC treated CEP chondrocytes. E Representative fluorescence images of dsDNA (green) and mitochondria (red) in the TBHP and TNF-α treated NP cells. F Representative western blotting images of COL2, MMP3, MMP13 and semi-quantitative analysis of band density in TBHP treated CEP chondrocytes with or without STING siRNA transfection. G Representative images of IHC of STING in CEP from 1-month aged, 3-month aged, 6-month-aged and 16-month-aged mice. Quantitative analysis of STING-positive chondrocytes as a proportion of the total chondrocytes. H Representative images of IHC of STING in CEP from mice after 1month, 2 months and 3 months after LSI surgery (n = 5, scale bar = 100 μm). Quantitative analysis of STING-positive chondrocytes as a proportion of the total chondrocytes (scale bar = 50 μm). Data are shown as the mean ± SD of at least three independent experiments. The P value is indicated by stars: *P < 0.05, **P < 0.01, ***P < 0.001, ****P < 0.0001. (For interpretation of the references to colour in this figure legend, the reader is referred to the Web version of this article.)

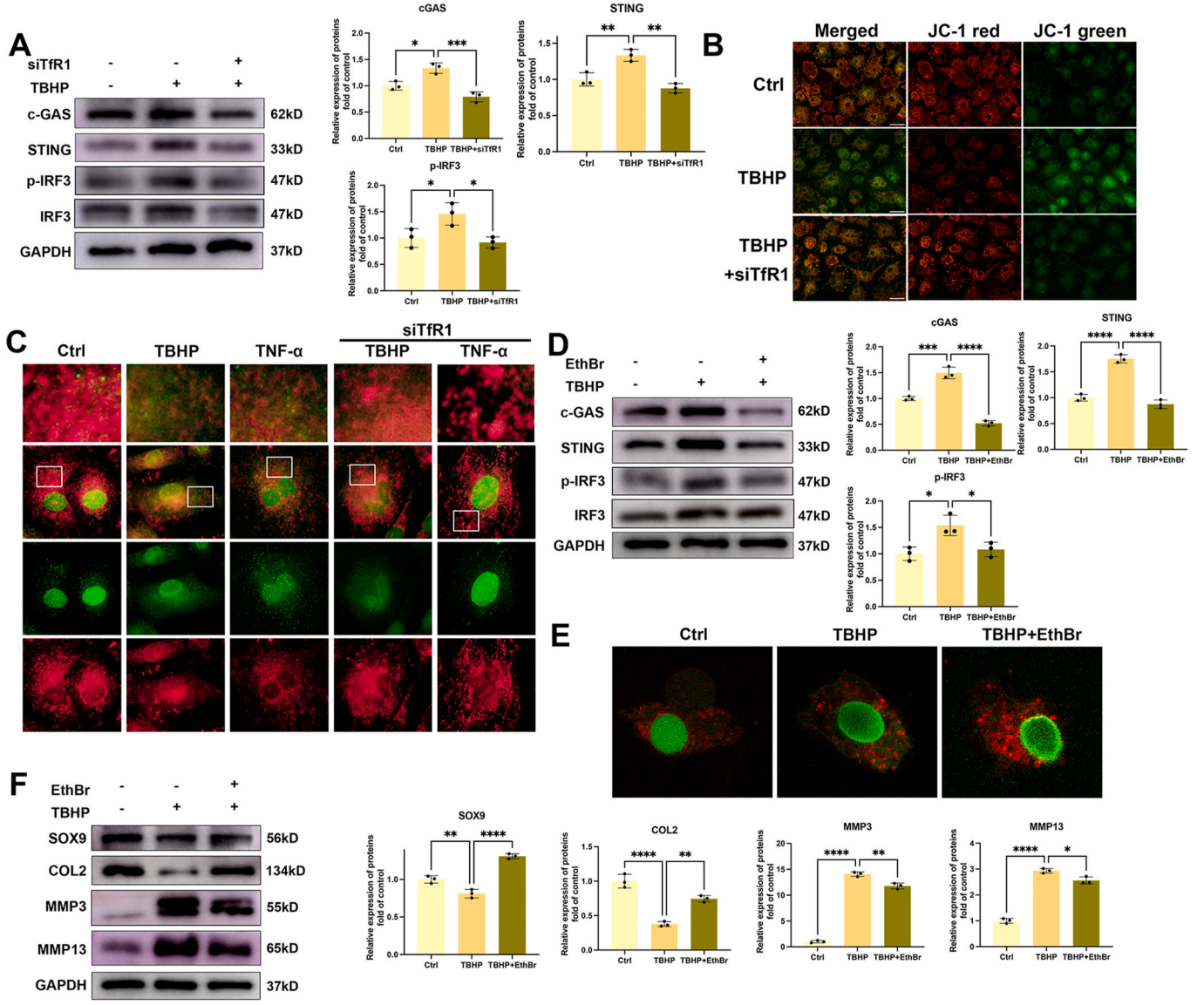

Fig. 6. TfR1 mediated mtDNA release plays essential roles in the cGAS-STING activation and CEP chondrocytes degeneration. A Representative western blotting images of cGAS, STING, p-IRF3, IRF3 and semi-quantitative analysis of band density in TBHP treated CEP chondrocytes with or without TfR1 siRNA transfection. B Mitochondrial membrane potential (MMP) was detected by fluorescence after chondrocytes were incubated with JC-1. Red fluorescence represents JC-1 aggregates in healthy mitochondria, while green fluorescence is emitted by JC-1 monomers, representing MMP dissipation. Merged images exhibit co-localization of JC- 1 aggregates and monomers. C Representative fluorescence images of dsDNA (green) and mitochondria (red) in the TBHP and TNF-α treated CEP chondrocytes with or without TfR1 siRNA transfection. scale bars = 50 μm. D CEP chondrocytes were pretreated with ethidium bromide 48h, then 100 μM TBHP was added and western blot was conducted to examine cGAS, STING, p-IRF3, IRF3 proteins expression. The band density was quantified and normalized to control. E Representative fluorescence images of dsDNA (green) and mitochondria (red) in the TBHP and EthBr treated CEP chondrocytes. F Representative western blotting images of SOX9, COL2, MMP3, MMP13 and semi-quantitative analysis of band density in TBHP and EthBr treated CEP chondrocytes. Data are shown as the mean ± SD of at least three independent experiments. The P value is indicated by stars: *P < 0.05, **P < 0.01, ***P < 0.001, ****P < 0.0001. (For interpretation of the references to colour in this figure legend, the reader is referred to the Web version of this article.)

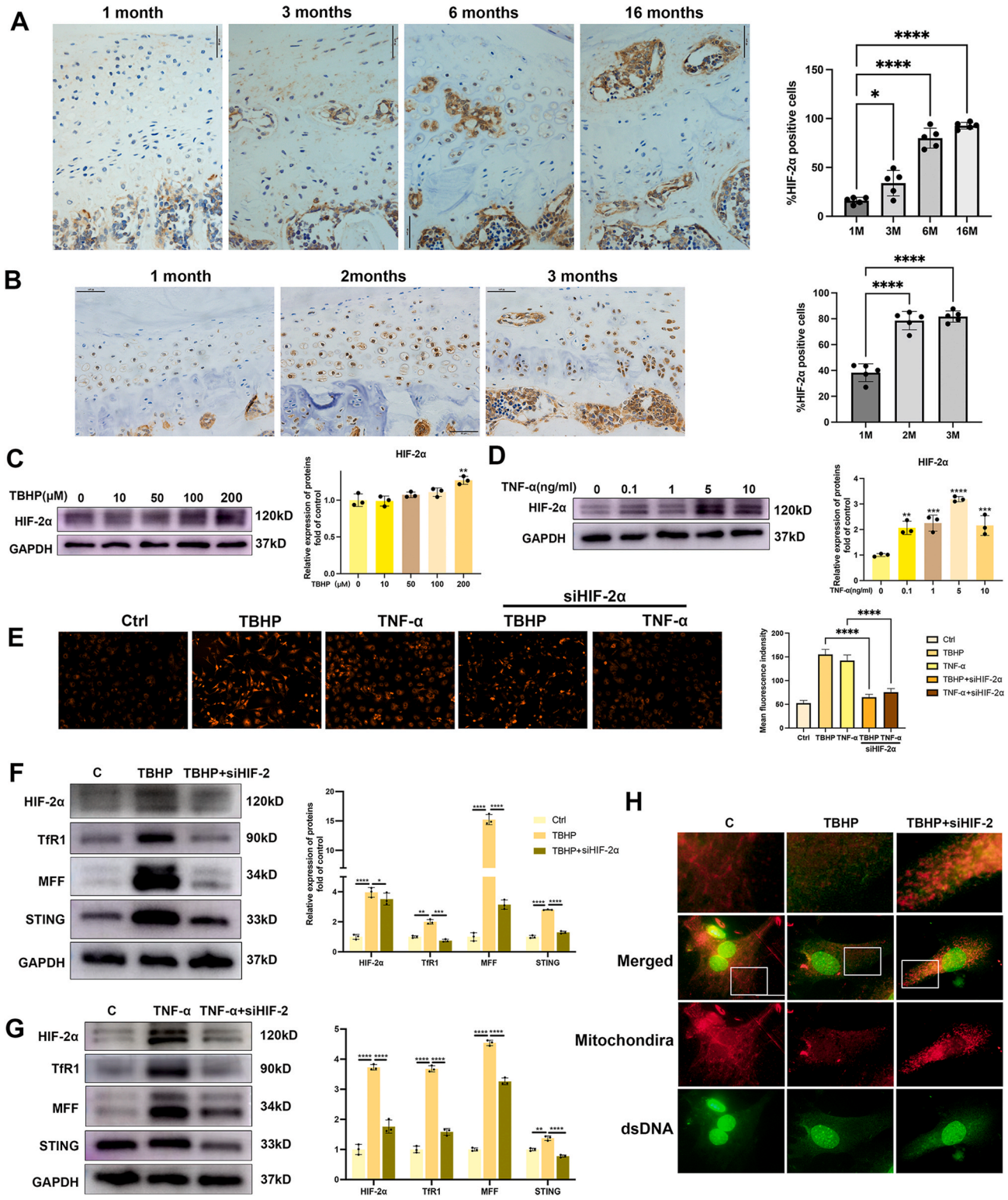

Fig. 7. TfR1 was upregulated in a HIF-2α dependent manner. A Representative images of IHC of HIF-2α in CEP from 1-month aged, 3-month aged, 6-month-aged and 16-month-aged mice. Quantitative analysis of TfR1-positive chondrocytes as a proportion of the total chondrocytes. B Representative images of IHC of HIF-2α in CEP from mice after 1month, 2 months and 3 months after LSI surgery (n = 5, scale bar = 50 μm). Quantitative analysis of TFR1-positive chondrocytes as a proportion of the total chondrocytes. C-D Representative western blotting images of HIF-2α and semi-quantitative analysis of band density in TBHP and TNF-α treated CEP chondrocytes. E Representative staining for ferrous ions in the indicated group and statistical analysis of fluorescence intensity. F-G Representative western blotting images of HIF-2α, TfR1, MFF, STING and semi-quantitative analysis of band density in TBHP and TNF-α treated CEP chondrocytes with or without HIF-2α siRNA transfection. H Representative fluorescence images of dsDNA (green) and mitochondria (red) in the TBHP treated CEP chondrocytes with or without HIF-2α siRNA transfection. Data are shown as the mean ± SD of at least three independent experiments. The P value is indicated by stars: *P < 0.05, **P < 0.01, ***P < 0.001, ****P < 0.0001. (For interpretation of the references to colour in this figure legend, the reader is referred to the Web version of this article.)

previous research confirmed iron overload is a significant risk factor for IDD progression [7], Nevertheless, the regulation of iron metabolism during the IDD progression remains unclear. In this study, we have shown that iron homeostasis in CEP chondrocytes is disrupted during IDD development. The pathological environment of IDD including oxidative stress and pro-inflammatory cytokines could promote iron influx by upregulating TfR1 expression in a HIF-2α dependent manner. Cellular iron overload could not only lead to chondrocytes ferroptosis and aggravate oxidative stress, but also activate the c-GAS/STING mediated innate immune response by promoting mitochondrial destruction and mtDNA release. To our best knowledge, this is the first comprehensive study investigating the connection between iron metabolism and IDD, along with its underlying mechanism. Our research suggests that preserving iron homeostasis by targeting TfR1 may represent a novel therapeutic approach for IDD.

Iron plays a dual role in human body, iron is essential for multiple cellular catabolic and anabolic processes, including DNA synthesis, respiration, and energy metabolism, Nevertheless, excessive labile iron concentrations can harm cells and organs by generating reactive oxygen species (ROS), consequently, iron homeostasis is delicately regulated [29]. TfR1 serves as the main cellular iron gate and plays important roles in controlling intracellular iron content [9]. Aging has a profound impact on iron homeostasis [30]. Aging is also the most important contributor to IDD [31]. Age-related iron accumulation has been demonstrated in multiple organs including the brain, liver and kidney [28]. In this study, we have, for the first time, confirmed that TfR1 expression in CEP increased during aging. Additionally, we created an IDD mouse model and observed an increase in TfR1 expression in the CEP 2 months after LSI surgery. These results suggest that iron homeostasis is disrupted during IDD progression, characterized by increased TFR1 expression and iron ions influx. To further elucidate the expression pattern of TfR1, primary CEP chondrocytes were isolated and treated with TBHP and TNF-α to mimic IDD pathogenic environment, we found that TBHP and TNF-α significantly promoted TfR1 expression and the iron influx in CEP chondrocytes. Chondrocytes are the only cell type in CEP and CEP Chondrocytes apoptosis plays essential roles in CEP degeneration [32]. Ferroptosis is a recently recognized iron dependent cell death program and increased iron concentration can render cells more susceptible to ferroptosis [33]. Our results also showed that TBHP and TNF-α promoted CEP chondrocytes ferroptosis. More importantly, our *in vitro* and *in vivo* results demonstrated that inhibition of TfR1 expression could attenuate CEP degeneration and IDD progression. These results demonstrated the important role of TfR1 in IDD pathogenesis.

Endplate osteochondritis is considered as one of the main causes of IDD, mtDNA has been demonstrated to be an important damage associated molecular pattern molecules (DAMPs), which can activate the cGAS-STING pathway, resulting in the migration and infiltration of inflammatory cells and the release of tissue inflammatory factors [34]. DNA damage plays an important role in many diseases, including progression of IDD. As a key element of many indispensable cellular players and co-factors, iron is required for oxygen transport and involved in the biosynthesis of collagen and many components of the mitochondrial electron transport chain [35]. Additionally, iron plays a vital role in the innate immune response to infections, recent studies have suggested that the process of ferroptosis is frequently accompanied by inflammation [36]. Intriguingly, our prior studies showed that iron overload in CEP chondrocytes could result in ferroptosis and mitochondrial dysfunction. The results of present study demonstrated that increased iron influx through TfR1 can trigger mitochondrial destruction and the mitochondrial mtDNA release. The inhibition of mtDNA using EthBr markedly reduced ECM degradation and suppressed the activation of cGAS-STING pathway, underscoring the pivotal role of mitochondrial destruction and mtDNA release in CEP degeneration [37]. Our findings imply a close association between ferroptosis and TfR1 with inflammatory mediators. The use of TfR1 siRNA can inhibit mtDNA release and the subsequent activation of cGAS-STING pathway.

The intervertebral disc, the largest avascular tissue in the human body, undergoes a range of changes as the body ages. One such change involves the calcification of the cartilage endplate, which, in turn, exacerbates the hypoxic microenvironment within the intervertebral disc [38]. Hypoxic stimulation can disrupt cellular iron metabolism and facilitate the deposition of iron in tissues. Under hypoxic conditions, cells enhance their uptake of iron to boost mitochondria energy production and enhance their tolerance to hypoxic environments [19,26]. In this study, we found that HIF-2α was upregulated in the CEP of IDD model mice and HIF-2α take parts in cellular iron metabolism regulation. The inhibition of HIF-2α results in decreased iron influx and a subsequent reduction in intracellular iron concentration. Moreover, the study underscores the HIF-2α dependent upregulation of TfR1, a vital element in cellular iron control. Inhibition of HIF-2α not only decreases TfR1 expression, but also mitigates the destruction of mitochondria. Recent research has also emphasized the role of elevated HIF expression in contributing to the IDD progression [39]. We hypothesize that the increased level of TfR1 in degenerated CEP is a protective mechanism that enables CEP chondrocytes to adapt to hypoxia conditions by promoting iron influx and energy production. However, the sustained and elevated presence of HIF-2α could potentially disrupt the delicate balance of iron metabolism by promoting TfR1 expression, lead to cellular iron overload and ferroptosis. These results underscore the intricate interplay between hypoxia and iron metabolism, providing new insights into the mechanisms of iron deposition in tissues and the broader context of diseases like IDD.

In summary, for the first time our study demonstrated that iron homeostasis dysfunction takes parts in IDD progression. IDD pathogenic conditions, such as oxidative stress and pro-inflammatory cytokines could disrupt CEP chondrocytes iron homeostasis via promoting TfR1 expression. Cellular iron overload would disrupt mitochondrial function, leading to oxidative stress and activating the mtDNA-cGAS-STING mediated inflammation. In addition, HIF-2α regulated TfR1 expression and played a role in iron homeostasis regulation. Our study indicate that maintaining iron homeostasis via targeting TfR1 may be a novel therapeutic strategy for IDD. Systemic inhibition of TFR1 using Fer-II could not constitute sufficient credible evidence to demonstrate the role of TfR1 in CEP degeneration and IDD progression. Further experiments with conditional gene knockout mice are need to offer direct role of TfR1 in CEP chondrocytes.

Data availability

The datasets generated during the current study are not publicly available due to the data also forming part of our ongoing study but are available from the corresponding author on reasonable request.

Funding

The present study was supported by the National Natural Science Foundation of China (grant no. 82002325), the Natural Science Foundation of Shandong Province (grant no. ZR2020QH075, ZR2021MH167, ZR2022LZY001 and ZR2023MH159). Municipal Innovation Plan of Clinical Medical Science and Technology of Jinan (202134043).

Ethics approval and consent to participate

The protocol of the animal model was approved by the Institutional Animal Care and Use Committee (IACUC) at Shandong provincial hospital affiliated to Shandong First Medical University (NSFC:NO.2022-816).

Author contributions

J.X.Z and C.X.G designed the experiments. J.X.Z., W.W.C., L.X.Y. and

S.Y.D. performed most of the experiments and analyzed the data. G.Z.P., H.X.N., Y.X.X. and W.H.R. partly performed the in vivo experiments. J. X.Z., W.W.C. and S.C. analyzed the data. J.X.Z. and W.W.C. wrote this manuscript.

Declaration of competing interest

The authors declare that they have no conflicts of interest.

References

[1] Dowdell J, Erwin M, Choma T, Vaccaro A, Iatridis J, Cho SK. Intervertebral disk degeneration and repair. Neurosurgery 2017;80:S46–54.
[2] Vergroesen PP, Kingma I, Emanuel KS, Hoogendoorn RJ, Welting TJ, van Royen BJ, et al. Mechanics and biology in intervertebral disc degeneration: a vicious circle. Osteoarthritis Cartilage 2015;23:1057–70.
[3] Haidar R, Mhaidli H, Musallam KM, Taher AT. The spine in beta-thalassemia syndromes. Spine 2012;37:334–9.
[4] Desigan S, Hall-Craggs MA, Ho CP, Eliahoo J, Porter JB. Degenerative disc disease as a cause of back pain in the thalassaemic population: a case-control study using MRI and plain radiographs. Skeletal Radiol 2006;35:95–102.
[5] Bywaters EG, Hamilton EB, Williams R. The spine in idiopathic haemochromatosis. Ann Rheum Dis 1971;30:453–65.
[6] Kati M, Tsironi M, Meletis I, Farmakis D, Giakoumis A, Aessopos A. Intervertebral disc calcification in a sickle cell thalassemia patient. Ann Hematol 2006;85:875–7.
[7] Wang W, Jing X, Du T, Ren J, Liu X, Chen F, et al. Iron overload promotes intervertebral disc degeneration via inducing oxidative stress and ferroptosis in endplate chondrocytes. Free Radic Biol Med 2022;190:234–46.
[8] Stockwell BR, Friedmann Angeli JP, Bayir H, Bush AI, Conrad M, Dixon SJ, et al. Ferroptosis: a regulated cell death nexus linking metabolism, redox biology, and disease. Cell 2017;171:273–85.
[9] Gammella E, Buratti P, Cairo G, Recalcati S. The transferrin receptor: the cellular iron gate. Metallomics 2017;9:1367–75.
[10] Kawabata H. Transferrin and transferrin receptors update. Free Radic Biol Med 2019;133:46–54.
[11] Li H, Choesang T, Bao W, Chen H, Feola M, Garcia-Santos D, et al. Decreasing TfR1 expression reverses anemia and hepcidin suppression in beta-thalassemic mice. Blood 2017;129:1514–26.
[12] Mietto BS, Jhelum P, Schulz K, David S. Schwann cells provide iron to axonal mitochondria and its role in nerve regeneration. J Neurosci 2021;41:7300–13.
[13] Feng H, Schorpp K, Jin J, Yozwiak CE, Hoffstrom BG, Decker AM, et al. Transferrin receptor is a specific ferroptosis marker. Cell Rep 2020;30:3411–34123 e7.
[14] Senyilmaz D, Virtue S, Xu X, Tan CY, Griffin JL, Miller AK, et al. Regulation of mitochondrial morphology and function by stearoylation of TFR1. Nature 2015;525:124–8.
[15] Kos N, Gradisnik L, Velnar T. A brief review of the degenerative intervertebral disc disease. Med Arch 2019;73:421–4.
[16] Li FC, Zhang N, Chen WS, Chen QX. Endplate degeneration may be the origination of the vacuum phenomenon in intervertebral discs. Med Hypotheses 2010;75:169–71.
[17] Jing X, Lin J, Du T, Jiang Z, Li T, Wang G, et al. Iron overload is associated with accelerated progression of osteoarthritis: the role of DMT1 mediated iron homeostasis. Front Cell Dev Biol 2020;8:594509.
[18] Ashinsky BG, Bonnevie ED, Mandalapu SA, Pickup S, Wang C, Han L, et al. Intervertebral disc degeneration is associated with aberrant endplate remodeling and reduced small molecule transport. J Bone Miner Res : the official journal of the American Society for Bone and Mineral Research 2020;35:1572–81.
[19] Goralska M, Fleisher LN, McGahan MC. Hypoxia induced changes in expression of proteins involved in iron uptake and storage in cultured lens epithelial cells. Exp Eye Res 2014;125:135–41.
[20] Renassia C, Peyssonnaux C. New insights into the links between hypoxia and iron homeostasis. Curr Opin Hematol 2019;26:125–30.
[21] Shao Y, Sun L, Yang G, Wang W, Liu X, Du T, et al. Icariin protects vertebral endplate chondrocytes against apoptosis and degeneration via activating Nrf-2/HO-1 pathway. Front Pharmacol 2022;13:937502.
[22] Byrne SL, Buckett PD, Kim J, Luo F, Sanford J, Chen J, et al. Ferristatin II promotes degradation of transferrin receptor-1 in vitro and in vivo. PLoS One 2013;8:e70199.
[23] Jing X, Wang Q, Du T, Zhang W, Liu X, Liu Q, et al. Calcium chelator BAPTAAM protects against iron overloadinduced chondrocyte mitochondrial dysfunction and cartilage degeneration. Int J Mol Med 2021;48.
[24] Yang RZ, Xu WN, Zheng HL, Zheng XF, Li B, Jiang LS, et al. Involvement of oxidative stress-induced annulus fibrosus cell and nucleus pulposus cell ferroptosis in intervertebral disc degeneration pathogenesis. J Cell Physiol 2021;236:2725–39.
[25] Zhang W, Li G, Luo R, Lei J, Song Y, Wang B, et al. Cytosolic escape of mitochondrial DNA triggers cGAS-STING-NLRP3 axis-dependent nucleus pulposus cell pyroptosis. Exp Mol Med 2022;54:129–42.
[26] Fuhrmann DC, Mondorf A, Beifuss J, Jung M, Brune B. Hypoxia inhibits ferritinophagy, increases mitochondrial ferritin, and protects from ferroptosis. Redox Biol 2020;36:101670.
[27] Ohnishi T, Iwasaki N, Sudo H. Causes of and molecular targets for the treatment of intervertebral disc degeneration: a review. Cells 2022;11.
[28] Gozzelino R, Arosio P. Iron homeostasis in health and disease. Int J Mol Sci 2016;17.
[29] Bresgen N, Eckl PM. Oxidative stress and the homeodynamics of iron metabolism. Biomolecules 2015;5:808–47.
[30] Kennish L, Attur M, Oh C, Krasnokutsky S, Samuels J, Greenberg JD, et al. Age-dependent ferritin elevations and HFE C282Y mutation as risk factors for symptomatic knee osteoarthritis in males: a longitudinal cohort study. BMC Muscoskel Disord 2014;15:8.
[31] Wang F, Cai F, Shi R, Wang XH, Wu XT. Aging and age related stresses: a senescence mechanism of intervertebral disc degeneration. Osteoarthritis Cartilage 2016;24:398–408.
[32] Ariga K, Miyamoto S, Nakase T, Okuda S, Meng W, Yonenobu K, et al. The relationship between apoptosis of endplate chondrocytes and aging and degeneration of the intervertebral disc. Spine 2001;26:2414–20.
[33] Dixon SJ, Lemberg KM, Lamprecht MR, Skouta R, Zaitsev EM, Gleason CE, et al. Ferroptosis: an iron-dependent form of nonapoptotic cell death. Cell 2012;149:1060–72.
[34] Zhang X, Wu J, Liu Q, Li X, Li S, Chen J, et al. mtDNA-STING pathway promotes necroptosis-dependent enterocyte injury in intestinal ischemia reperfusion. Cell Death Dis 2020;11:1050.
[35] Kuhn LC. Iron regulatory proteins and their role in controlling iron metabolism. Metallomics : integrated biometal science 2015;7:232–43.
[36] Li W, Feng G, Gauthier JM, Lokshina I, Higashikubo R, Evans S, et al. Ferroptotic cell death and TLR4/Trif signaling initiate neutrophil recruitment after heart transplantation. J Clin Invest 2019;129:2293–304.
[37] Guo Q, Zhu D, Wang Y, Miao Z, Chen Z, Lin Z, et al. Targeting STING attenuates ROS induced intervertebral disc degeneration. Osteoarthritis Cartilage 2021;29:1213–24.
[38] Huang Y, Wang Y, Wu C, Tian W. Elevated expression of hypoxia-inducible factor-2alpha regulated catabolic factors during intervertebral disc degeneration. Life Sci 2019;232:116565.
[39] Fujita N, Chiba K, Shapiro IM, Risbud MV. HIF-1alpha and HIF-2alpha degradation is differentially regulated in nucleus pulposus cells of the intervertebral disc. J Bone Miner Res : the official journal of the American Society for Bone and Mineral Research 2012;27:401–12.